Supporting information

Ni_xCu_{1-x}/CuO/$Ni(OH)_2$ as Highly Active and Stable Electrocatalysts for Oxygen Evolution Reaction

Xiaoqiang Wu,[1,*] Chaoyou Yong,[1] Xuguang An,[1] Qingquan Kong,[1] Weitang Yao,[1] Yong Wang,[2] Qingyuan Wang,[1,7] Yimin Lei,[3] Weiyin Li,[4] Zhiyang Xiang,[5] Liang Qiao,[2] Xiaonan Liu,[6]

[1]School of Mechanical Engineering, Chengdu University, Chengdu 610106, China,

E-mail: wuxiaoqiang@cdu.edu.cn (Wu Xiaoqiang)

[2]School of Physics, University of Electronic Science and Technology of China, Chengdu 610054, China, liang.qiao@uestc.edu.cn(Qiao Liang)

[3]School of Advanced Materials and Nanotechnology, Xidian University 710726 Xi'An, China

[4]Sch Elect & Informat Engn, North Minzu Univ, Yinchuan 750021, China

[5]Dongfang Turbine Co.,Ltd. Deyang 618000, China

[6]College of Chemical Engineering, Sichuan University of Science and Engineering, Zigong 643000, China

[7]Institute for Advanced Study, Chengdu University, Chengdu 610106, China

1. Polarization curves and electrodeposition of the of Ni_xCu_{1-x} /CuO/$Ni(OH)_2$

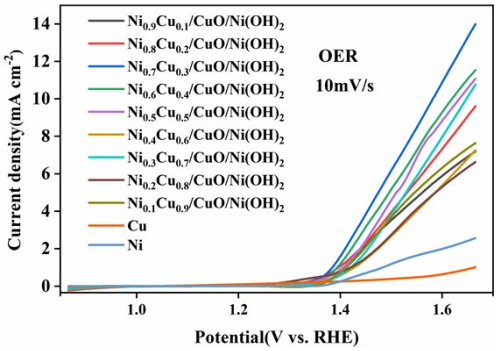

Figure S1. Polarization curves of the OER.

Fig.S1 is the LSV curve of Ni_xCu_{1-x}/CuO/$Ni(OH)_2$ tested at a scanning rate of 10mV/s. It can be seen from the figure that the initial potential and overpotential of $Ni_{0.7}Cu_{0.3}$/CuO/$Ni(OH)_2$ are higher than those of the other proportions. Under the same potential, the current density is higher.

$$m_{Cu} = \frac{\frac{Q}{2e} \times ((1 - x)/10)}{N_A} \times M_{Cu} \quad (1)$$

$$m_{Ni} = \frac{\frac{Q}{2e} \times (x/10)}{N_A} \times M_{Ni} \quad (2)$$

In equations (1) and (2): Q is the total amount of charge deposited on the glassy carbon (calculated by integrating the electrodeposition curve), and e is the amount of charge of an electron (E = 1.6×10^{-19} C). N_A is Avogadro's constant (N_A =6.022×10^{23}), and M_{Ni} and M_{Cu} are the molar masses of Ni and Cu atoms (M_{Ni} =58.7 g mol^{-1}, M_{Cu}=63.5 g mol^{-1}), respectively. $m=m_{Ni}+m_{Cu}$.

2.TGA analysis of Ni_xCu_{1-x}/CuO/$Ni(OH)_2$ electrocatalysts and XRD of GS

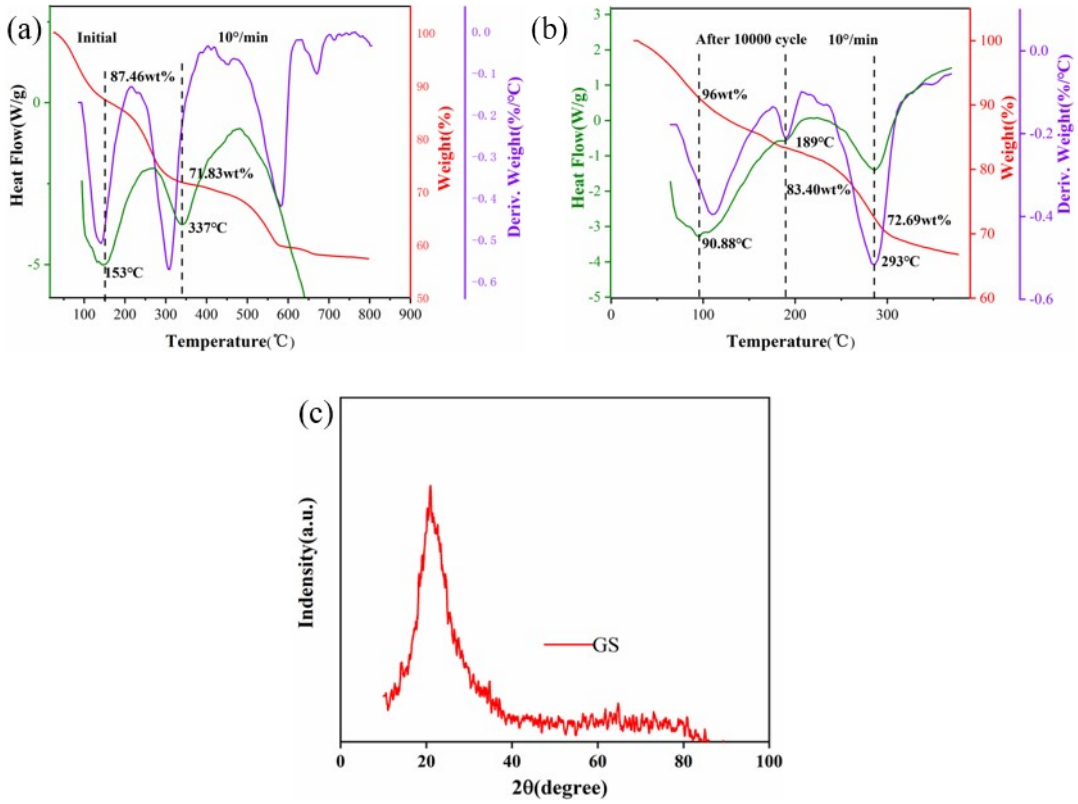

Figure S2. (a-b) Comparison of different heating rates and after 10000 cycles of CV decay, **(c)** XRD of glass slide.

The pyrolysis process of $Ni_{0.7}Cu_{0.3}$/CuO/$Ni(OH)_2$ at a heating rate of 10 ℃ / min was obtained by thermogravimetric analysis. **Fig.S2(a)** is the thermogravimetric analysis of $Ni_{0.7}Cu_{0.3}$/CuO/$Ni(OH)_2$ before the activity test. The exothermic peak of the first stage is at 153 °C and the exothermic peak of the second stage is at 337 ℃. Compared with the exothermic peak of the heating rate of 5 ℃/ min, They' re all offset in the positive direction. It shows that the heating rate has an effect on the location of the exothermic peak. **Fig.S2(b)** is thermogravimetric analysis of $Ni_{0.7}Cu_{0.3}$/CuO/$Ni(OH)_2$ after 10000 CV cycle. The exothermic peak of the first stage was at 90.88 degrees Celsius, and the exothermic peak of the second stage was at 293

degrees Celsius, which moved in a negative direction compared with the initial exothermic peak. This indicates that the position changes after 10000 CV cycles.

3.XPS analysis of $Ni_xCu_{1-x}/CuO/Ni(OH)_2$ electrocatalysts

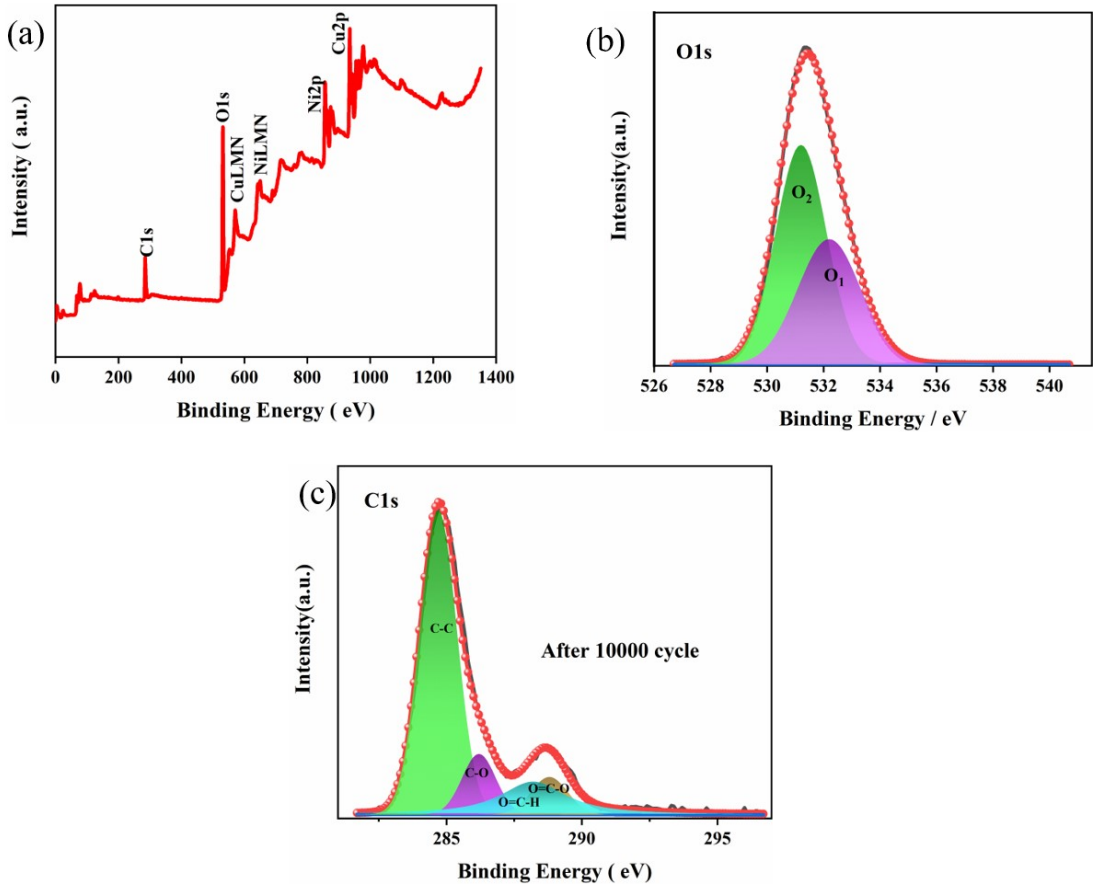

Figure S3. The XPS spectrum of $Ni_{0.7}Cu_{0.3}/CuO/Ni(OH)_2$ after 10000 cycle (a) and high- resolution XPS spectra of (b) Ni 2p, (c) C1s, (d) O1s.

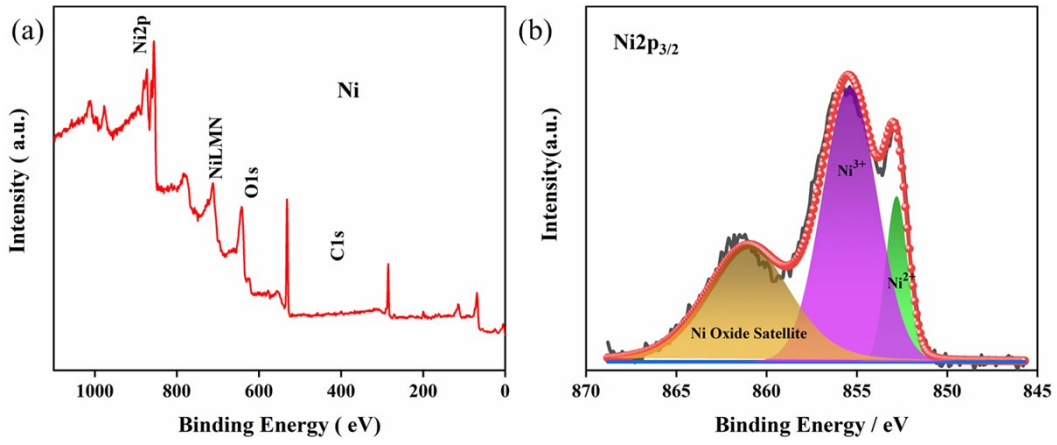

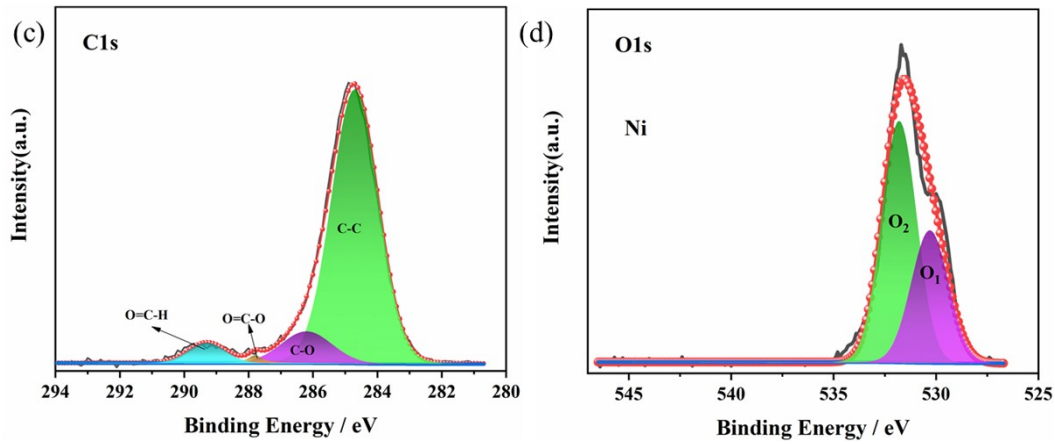

Figure S4. XPS spectra of Ni electrocatalyst (a) and high- resolution XPS spectra of (b) Ni 2p, (c) C1s, (d) O1s.

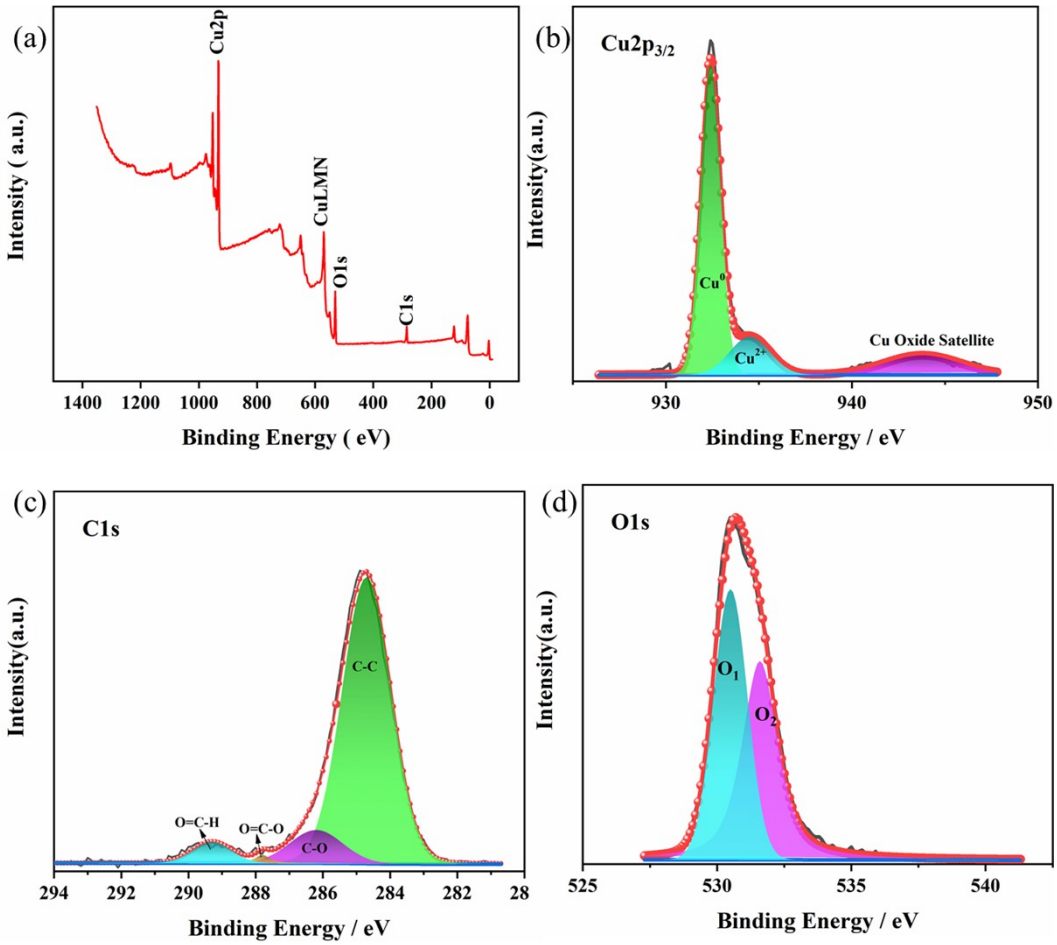

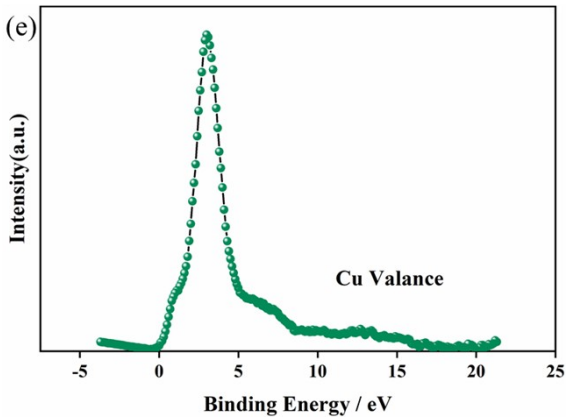

Figure S5. XPS spectra of Cu electrocatalyst (a) and high- resolution XPS spectra of (b) Cu 2p, (c) C1s, (d) O1s, (e) Valence band spectra of Cu.

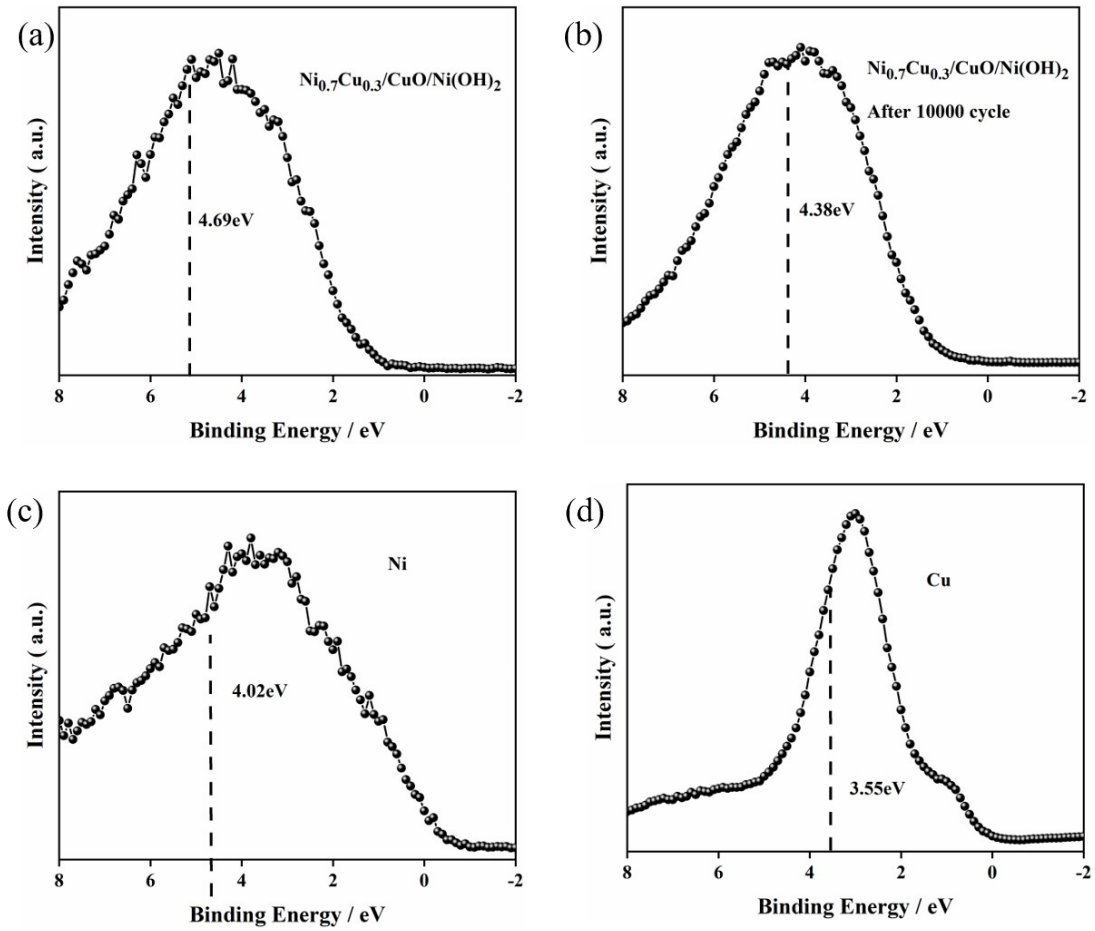

Figure S6. The d-band center position obtained from the valence-band spectra of different materials relative to the Fermi level. (a) $Ni_{0.7}Cu_{0.3}/CuO/Ni(OH)_2$, (b) $Ni_{0.7}Cu_{0.3}/CuO/Ni(OH)_2$ after 10000 cycle , (c) Ni, (d) Cu.

The position of the center of the valence band is given by $\int N(\varepsilon)\varepsilon d\varepsilon / \int N(\varepsilon) d\varepsilon$,

where $N(\varepsilon)$ is the DOS or, in our case, the XPS-intensity after background subtraction[1-2]. **Fig.S6(a)** is the valence band spectrum of $Ni_{0.7}Cu_{0.3}/CuO/Ni(OH)_2$, The position of the center of the valence band is 4.69 eV. **Fig.S6(b)** is the valence band spectrum of $Ni_{0.7}Cu_{0.3}/CuO/Ni(OH)_2$ after 10000 cycle, The position of the center of the valence band is 4.38 eV . **Fig.S6(c)** is the valence band spectrum of Ni after 10000 cycle, The position of the center of the valence band is 4.02 eV. **Fig.S6(d)** is the valence band spectrum of Cu after 10000 cycle, The position of the center of the valence band is 3.55 eV. It shows that after alloying, the center of D band is in a positive direction. At the same time, after 10,000 cycle, the center of Ni D-band moves to a negative direction, indicating that the catalytic performance is weakened.

4.TEM and SEM analysis of $Ni_xCu_{1-x}/CuO/Ni(OH)_2$ electrocatalysts

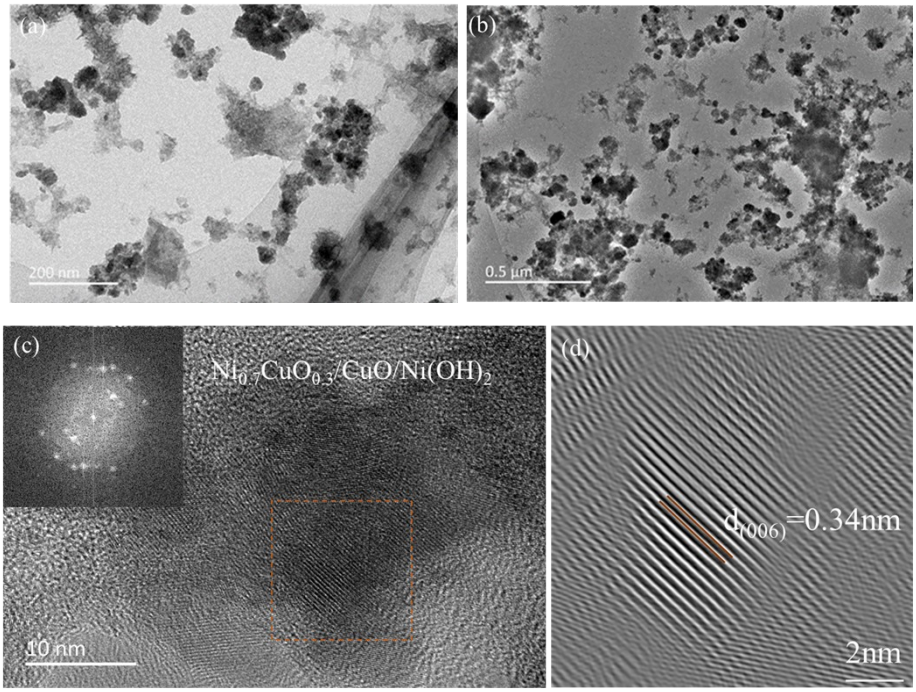

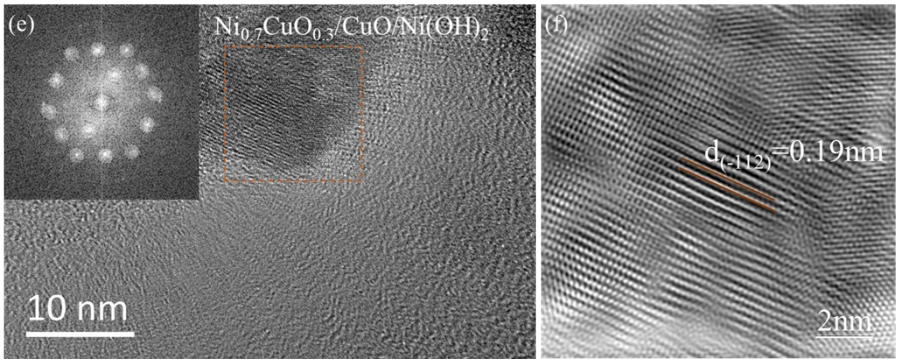

Figure S7. (a-f) Lattice information under TEM of $Ni_{0.7}Cu_{0.3}$/CuO/$Ni(OH)_2$.

Fig.S7 (a-b) shows the morphology of Ni in other regions under TEM, and it can be seen that the sample is many small clusters. **Fig.S7(c-f)** is the lattice information diagram of a region of Ni, where $d_{(006)}$=0.34nm, indicating the presence of NiOOH, which is conducive to oxygen precipitation reaction. $d_{(-112)}$=0.19nm, indicating the presence of CuO, which also contributes to the oxygen precipitation reaction.

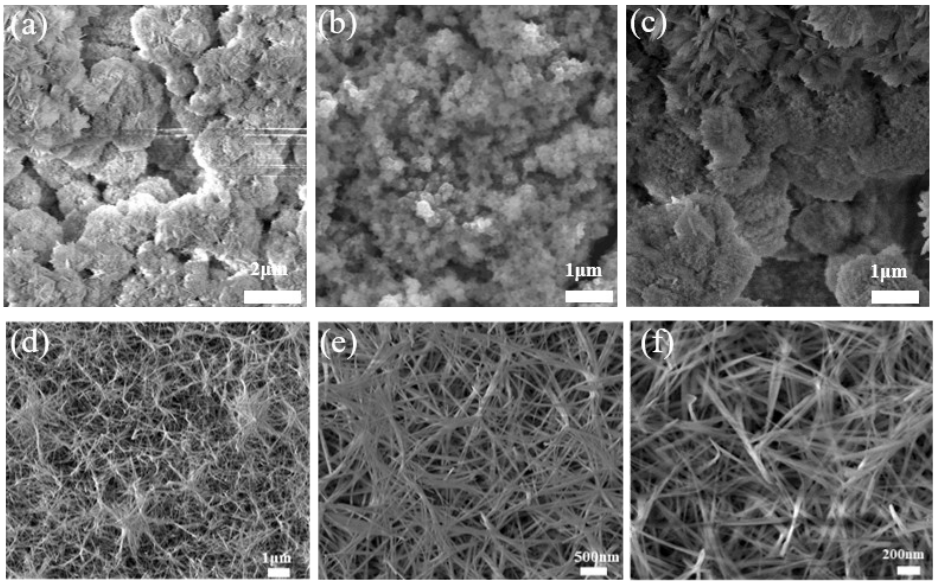

Figure S8. SEM image of $Ni_{0.7}Cu_{0.3}/CuO/Ni(OH)_2$ composite prepared by a-c)i-t, d-f) LSV deposition method.

As shown in **Fig.S8**, the morphology of $Ni_{0.7}Cu_{0.3}/CuO/Ni(OH)_2$ deposited by linear scanning voltammetry (LSV) with the magnification of 1 μ m,500m and 200m can be seen as fine strip morphology. Compared with the morphology of $Ni_{0.7}Cu_{0.3}/CuO/Ni(OH)_2$ deposited by it, there are more pores and poor stability.

5. Electrocatalyst activity of $Ni_{0.7}Cu_{0.3}/CuO/Ni(OH)_2$

Table S1. The initial potential and overpotential of different NiCu atomic ratios and the corresponding current density when the potential was 1.5V.

$Ni_xCu_{1-x}/CuO/Ni(OH)_2$	Onset potential/mV	Overpotential (vs. 3.33 A g^{-1})/mV	Current density (vs.1.5V)/A g^{-1}
$Ni_{0.1}Cu_{0.9}/CuO/Ni(OH)_2$	144.3	189	10.24
$Ni_{0.2}Cu_{0.8}/CuO/Ni(OH)_2$	163.3	203	7.62
$Ni_{0.3}Cu_{0.7}/CuO/Ni(OH)_2$	179.3	199	10.59
$Ni_{0.4}Cu_{0.6}/CuO/Ni(OH)_2$	174.3	208	7.40
$Ni_{0.5}Cu_{0.5}/CuO/Ni(OH)_2$	152.3	183	12.74
$Ni_{0.6}Cu_{0.4}/CuO/Ni(OH)_2$	140.0	170	14.36
$Ni_{0.7}Cu_{0.3}/CuO/Ni(OH)_2$	136.6	160	17.14
$Ni_{0.8}Cu_{0.2}/CuO/Ni(OH)_2$	158.3	177	10.95
$Ni_{0.9}Cu_{0.1}/CuO/Ni(OH)_2$	143.3	188	9.78
Ni	145.3	272	3.28
Cu	358.3	/	1.07

Table S2. Mass activity ratio conversion

Current density	Quality of **Ref.3** [3]	Mass activity of **Ref.3**	Overpotential of **Ref.3**	Overpotential of this work (vs. 3.33 A g^{-1})
10 mA cm^{-2}	3 mg cm^{-2}	3.33 A g^{-1}	259 mV	160 mV

The current density of 10 mA cm^{-2} of **Ref.3** was converted into mass specific activity, and the potential of $Ni_{0.7}Cu_{0.3}/CuO/Ni(OH)_2$ with mass specific activity of 3.33A g^{-1} was obtained (160 mV).

The ECSA of the electrocatalyst was calculated using eqn. (3) The inset plot in **Fig.5(e)** is the cathodic and anodic charging currents measured at $0.6V_{RHE}$~$0.72V_{RHE}$ and plotted as a function of scan rate. The C_{dl} was determined from the average of the cathodic and anodic slopes. Here, the electrochemical double-layer capacitance of $Ni_{0.7}Cu_{0.3}/CuO/Ni(OH)_2$ complex oxides was estimated to be 0.305 mF. Cs is the specific capacitance of the electrocatalyst per unit area under identical electrolyte conditions. Its value has been reported between 0.022 to 0.130 mF cm^{-2} in alkaline solution. In this study, value of Cs was taken to be 0.040 mF cm^{-2} based on reported values.[4]

$$ECSA = Cdl/Cs \tag{3}$$

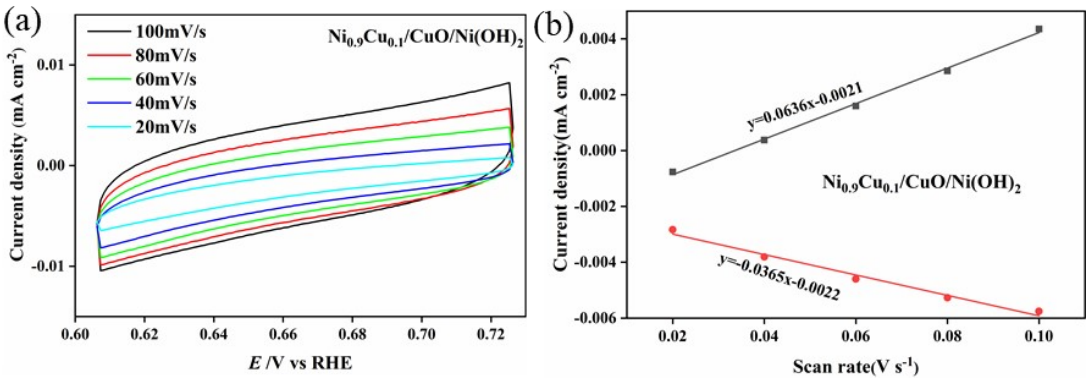

Figure S9(a-b). (a)CV cycle test curves of $Ni_{0.9}Cu_{0.1}/CuO/Ni(OH)_2$ with different ratios. (b) Digrams of anode and cathode current densities and scanning velocity of CV curves of $Ni_{0.9}Cu_{0.1}/CuO/Ni(OH)_2$.

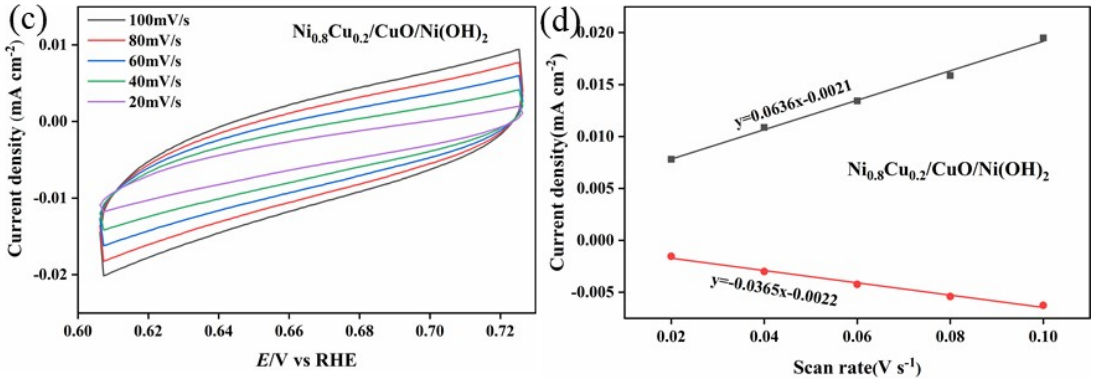

Figure S9(c-d). (c)CV cycle test curves of $Ni_{0.8}Cu_{0.2}/CuO/Ni(OH)_2$ with different ratios. (d) Digrams of anode and cathode current densities and scanning velocity of CV curves of $Ni_{0.8}Cu_{0.2}/CuO/Ni(OH)_2$.

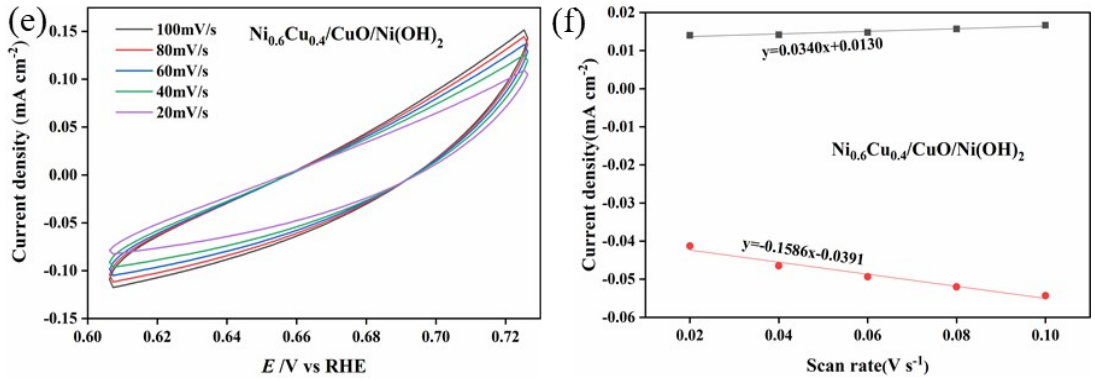

Figure S9(e-f). (e)CV cycle test curves of $Ni_{0.6}Cu_{0.4}/CuO/Ni(OH)_2$ with different ratios. (f) Digrams of anode and cathode current densities and scanning velocity of CV curves of $Ni_{0.6}Cu_{0.4}/CuO/Ni(OH)_2$.

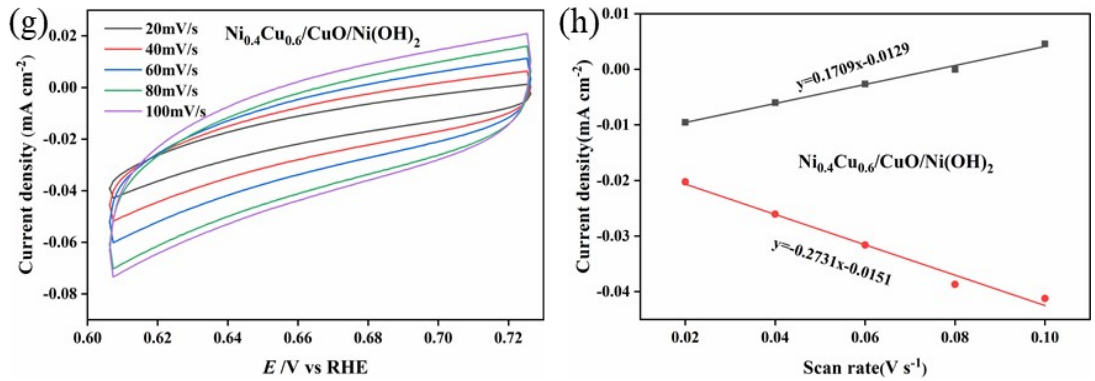

Figure S9(g-h). (g)CV cycle test curves of $Ni_{0.4}Cu_{0.6}/CuO/Ni(OH)_2$ with different

ratios. (h) Digrams of anode and cathode current densities and scanning velocity of CV curves of $Ni_{0.4}Cu_{0.6}/CuO/Ni(OH)_2$.

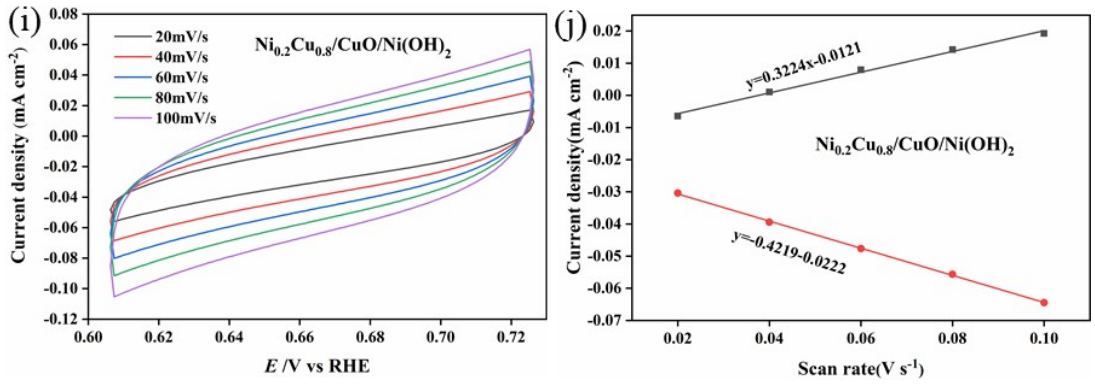

Figure S9(i-j). (i)CV cycle test curves of $Ni_{0.2}Cu_{0.8}/CuO/Ni(OH)_2$ with different ratios. (j) Digrams of anode and cathode current densities and scanning velocity of CV curves of $Ni_{0.2}Cu_{0.8}/CuO/Ni(OH)_2$.

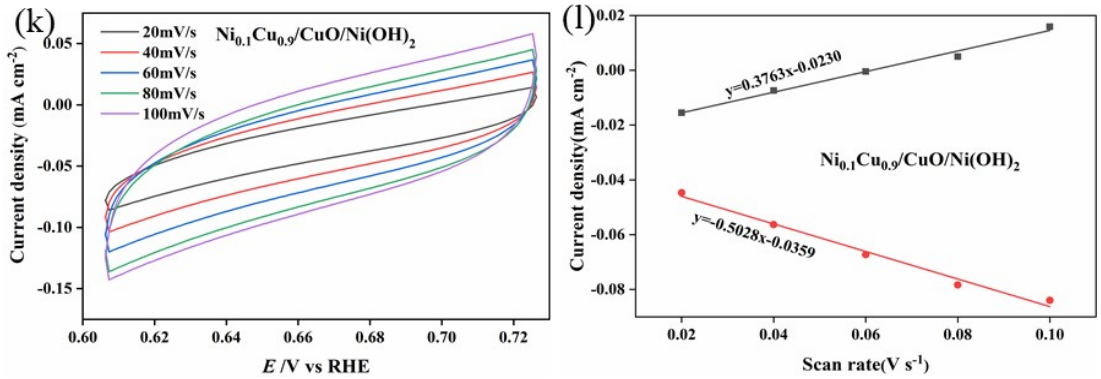

Figure S9(k-l). (k)CV cycle test curves of $Ni_{0.1}Cu_{0.9}/CuO/Ni(OH)_2$ with different ratios. (l) Digrams of anode and cathode current densities and scanning velocity of CV curves of $Ni_{0.1}Cu_{0.9}/CuO/Ni(OH)_2$.

Fig. S9 (a-l) shows the CV curves of $Ni_xCu_{1-x}/CuO/Ni(OH)_2$ with different ratios of 0.60 V_{RHE} to 0.72 V_{RHE} and the relationship between anode and cathode current densities and sweep rates at 0.66 V_{RHE} potential. C_{dl} was obtained by calculating the absolute difference of the current density between anode and cathode, and Cs was 0.04mF cm^{-2}. The ECSA value of $Ni_xCu_{1-x}/CuO/Ni(OH)_2$ with different ratios could be obtained by Formula 1. By comparing their values, they represented the size of the

electrochemical active surface area. $Ni_xCu_{1-x}/CuO/Ni(OH)_2$ with good catalytic performance can be determined by evaluating their activity by electrochemical activity surface area.

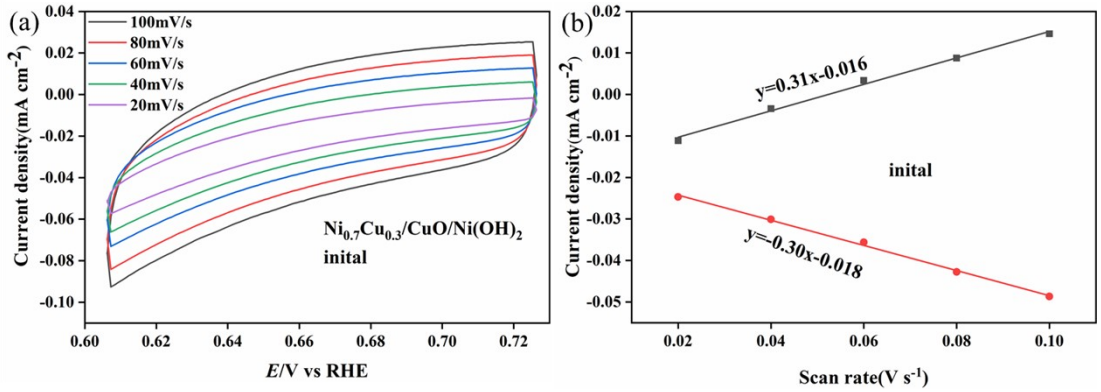

Figure S10(a-b). (a) CV curves of $Ni_{0.7}Cu_{0.3}/CuO/Ni(OH)_2$ at different scanning rates in the active region before the CV cycle, (b) Digrams of anode and cathode current densities and scanning velocity of CV curves of $Ni_{0.7}Cu_{0.3}/CuO/Ni(OH)_2$ before the CV cycle.

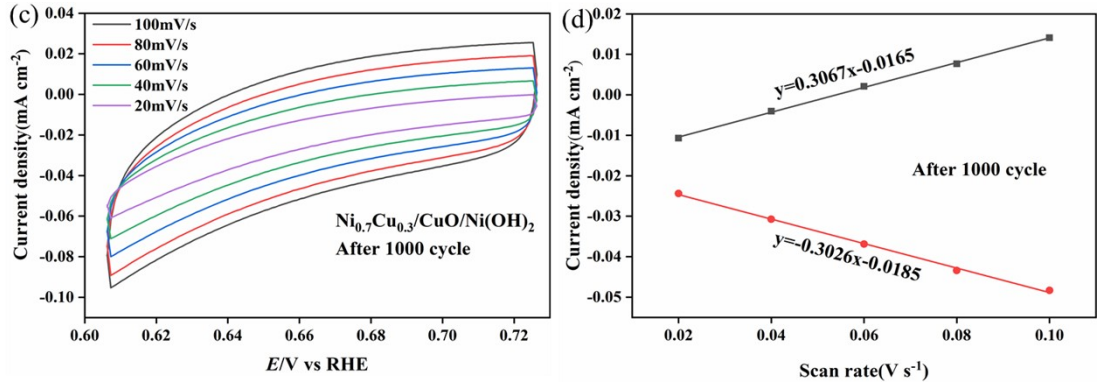

Figure S10(c-d). (c) CV curves of $Ni_{0.7}Cu_{0.3}/CuO/Ni(OH)_2$ at different scanning rates in the active region after 1000 CV cycle, (d) Digrams of anode and cathode current densities and scanning velocity of CV curves of $Ni_{0.7}Cu_{0.3}/CuO/Ni(OH)_2$ after 1000 CV cycle.

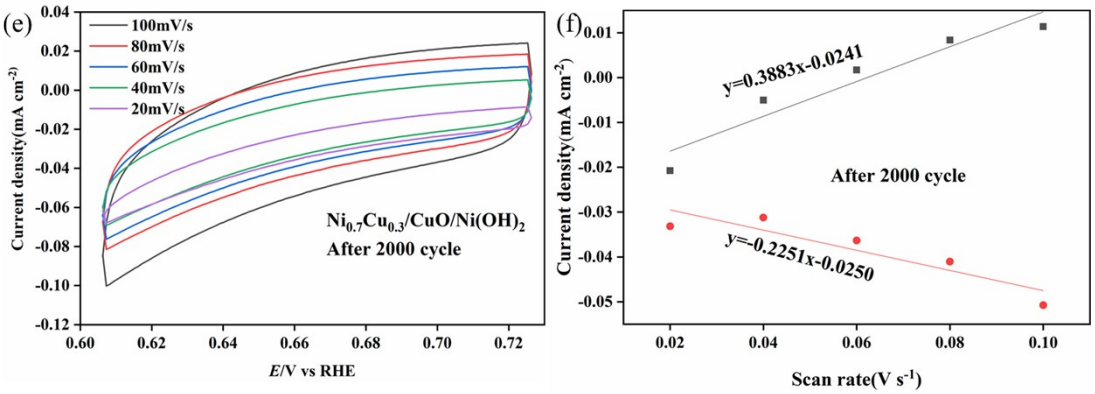

Figure S10(e-f). (e) CV curves of $Ni_{0.7}Cu_{0.3}/CuO/Ni(OH)_2$ at different scanning rates in the active region after 2000 CV cycle, (f) Digrams of anode and cathode current densities and scanning velocity of CV curves of $Ni_{0.7}Cu_{0.3}/CuO/Ni(OH)_2$ after 2000 CV cycle.

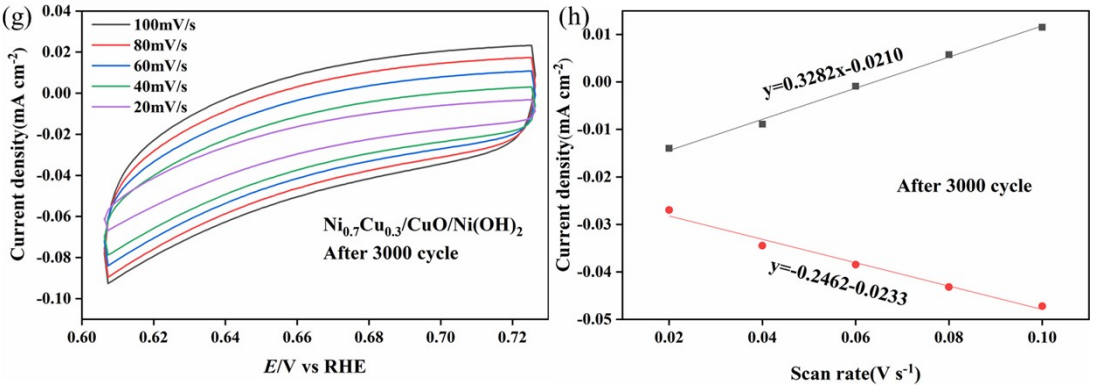

Figure S10(g-h). (g) CV curves of $Ni_{0.7}Cu_{0.3}/CuO/Ni(OH)_2$ at different scanning rates in the active region after 3000 CV cycle, (f) Digrams of anode and cathode current densities and scanning velocity of CV curves of $Ni_{0.7}Cu_{0.3}/CuO/Ni(OH)_2$ after 3000 CV cycle.

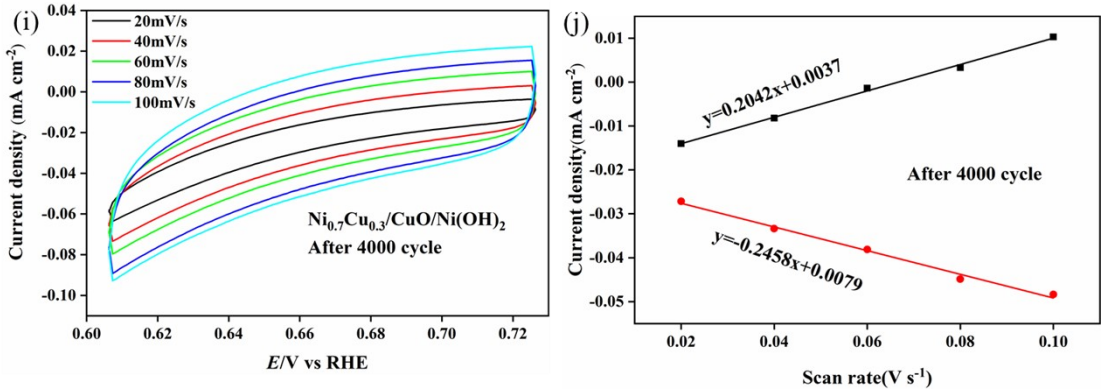

Figure S10(i-j). (g) CV curves of $Ni_{0.7}Cu_{0.3}/CuO/Ni(OH)_2$ at different scanning rates in the active region after 4000 CV cycle, (f) Digrams of anode and cathode current

densities and scanning velocity of CV curves of $Ni_{0.7}Cu_{0.3}/CuO/Ni(OH)_2$ after 4000 CV cycle.

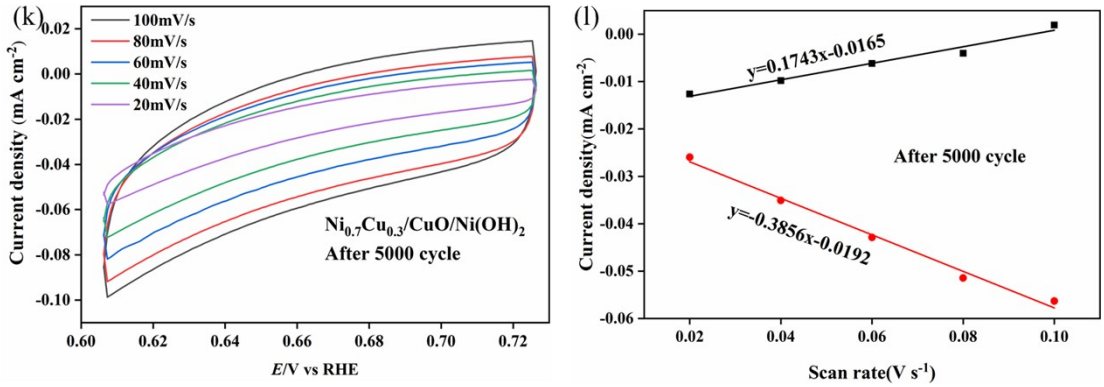

Figure S10(k-l). (g) CV curves of $Ni_{0.7}Cu_{0.3}/CuO/Ni(OH)_2$ at different scanning rates in the active region after 5000 CV cycle, (f) Digrams of anode and cathode current densities and scanning velocity of CV curves of $Ni_{0.7}Cu_{0.3}/CuO/Ni(OH)_2$ after 5000 CV cycle.

As shown in **Fig.S10 (a-l)**, the CV curve of the attenuation of $Ni_{0.7}Cu_{0.3}/CuO/Ni(OH)_2$ at the active interval of 0.60 V_{RHE}-0.72 V_{RHE} after 1000 CV and the relationship between the anode and cathode current density and sweep rate when the potential was 0.66 V_{RHE}. C_{dl} was obtained by calculating the absolute difference of current density between anode and cathode, and C_S was 0.04mF cm^{-2}. The ECSA value of $Ni_{0.7}Cu_{0.3}/CuO/Ni(OH)_2$ after 1000 cycles could be obtained by formula 1. The durability of $Ni_{0.7}Cu_{0.3}/CuO/Ni(OH)_2$ can be evaluated, as shown in Figure 6 (a). It can be seen that the change trend is small, indicating that the durability of $Ni_{0.7}Cu_{0.3}/CuO/Ni(OH)_2$ is good.

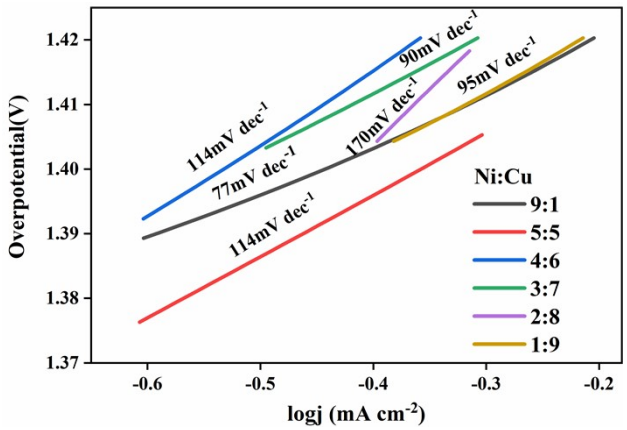

Figure S11. Comparison of the remaining Tafer slope sizes.

Fig.S11 shows the Tafel curves of other ratios outside the main body, in which the maximum value is $Ni_{0.2}Cu_{0.8}/CuO/Ni(OH)_2$, and the minimum value is $Ni_{0.9}Cu_{0.1}/CuO/Ni(OH)_2$. However, compared with $Ni_{0.7}Cu_{0.3}/CuO/Ni\ (OH)_2$, the Tafel slope value is still larger. It can be concluded that $Ni_{0.7}Cu_{0.3}/CuO/Ni\ (OH)_2$ has better OER activity.

The Tafel slope is the important parameter to explain the electrocatalytic activity and kinetics of a given reaction and can be expressed as follows. Where η is the overpotential, j is the current density, and b is the Tafel slope.

$$\eta = a + blogj \tag{3}$$

Tab.S3 the Ni and Cu content of initial- and used- $Ni_{0.7}Cu_{0.3}/CuO/Ni(OH)_2$

content	Initial (atomic %)	Used (atomic %)	Initial (Area eV)	Used (Area eV)
Ni content	11.53%	9.67%	162525.90	115770.05
Cu content	12.88%	9.17%	168502.28	92687.84

Tab.S4 The Ni and Cu content of $Ni_xCu_{1-x}/CuO/Ni(OH)_2$

$Ni_xCu_{1-x}/CuO/Ni(OH)_2$	Ni (Atomic%)	Cu (Atomic%)
$Ni_{0.9}Cu_{0.1}/CuO/Ni(OH)_2$	88.09%	11.91%
$Ni_{0.8}Cu_{0.2}/CuO/Ni(OH)_2$	80.67%	19.33%
$Ni_{0.7}Cu_{0.3}/CuO/Ni(OH)_2$	69.20%	30.80%
$Ni_{0.6}Cu_{0.4}/CuO/Ni(OH)_2$	58.03%	41.97%
$Ni_{0.5}Cu_{0.5}/CuO/Ni(OH)_2$	53.98%	46.02%
$Ni_{0.4}Cu_{0.6}/CuO/Ni(OH)_2$	41.22%	58.78%
$Ni_{0.3}Cu_{0.7}/CuO/Ni(OH)_2$	32.51%	67.49%
$Ni_{0.2}Cu_{0.8}/CuO/Ni(OH)_2$	18.44%	81.56%
$Ni_{0.1}Cu_{0.9}/CuO/Ni(OH)_2$	10.93%	89.07%
Ni	100%	0%
Cu	0%	100%

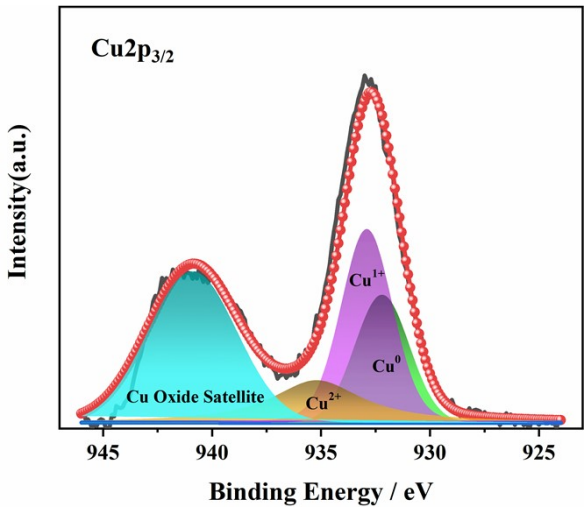

Figure S12. high- resolution XPS spectra of Cu 2p

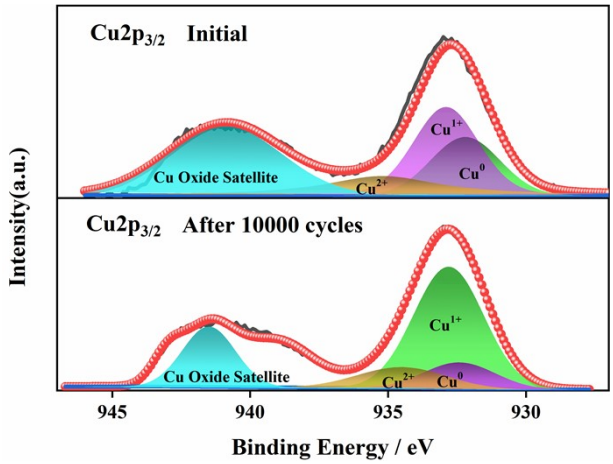

Figure S13. the initial-$Ni_{0.7}Cu_{0.3}$/CuO/$Ni(OH)_2$ and long-term used $Ni_{0.7}Cu_{0.3}$/CuO/$Ni(OH)_2$ of high-resolution XPS spectra of Cu2p

Tab.S5 Auger spectra of Cu in different valence states

Reference	type	Cu LMM/eV
Ref.6[5]	Cu	918.7
Ref.7[6-9]	Cu_2O	916.9
Ref.8[10-11]	CuO	917.9

References

1 S.J. Hwang, S.K. Kim, J.G. Lee, S.C. Lee, J.H. Jang, P. Kim, T.H. Lim, Y.E. Sung, S.J. Yoo, *J. Am. Chem. Soc.,* 2012, **134**, 19508-19511.

2 W.P. Zhou, A. Lewera, R. Larsen, R.I. Masel, P.S. Bagus, A. Wieckowski, *J. Phys. Chem. B,* 2006, **110**, 13393-13398.

3 H. Liu, Z. Guo, J. Lian, *J. Solid. State. Chem.,* 2021, **293**.

4 X. Cao, Y. Hong, N. Zhang, Q. Chen, J. Masud, M.A. Zaeem, M. Nath, *ACS Catal.,* 2018, **8**, 8273-8289.

5 C.D. Wagner, J.F. Moulder, L. Davis, W. Riggs, *Hand Book of X-Ray Photoelectron Spectroscopy,* 2008.

6 T. Shinagawa, G.O. Larrazábal, A.J. Martín, F. Krumeich, J. Pérez-Ramírez, *ACS Catal.,* 2018, **8**, 837-844.

7 John, P., Tobin, and, W., Hirschwald, and, J., Cunningham, *Appl. Surf. Sci.,* 1983.

8 M.T. Anthony, M.P. Seah, *Surf. Interface Anal.,* 1984, **6**, 107-115.

9 D. Ruano, J. Cored, C. Azenha, V. Pérez-Dieste, A. Mendes, C. Mateos-Pedrero, P. Concepción, *ACS Catal.,* 2019, **9**, 2922-2930.

10 A.K.S. Clemens, A. Shishkin, P.A. Carlsson, M. Skoglundh, F.J. Martínez-Casado, Z. Matěj, O. Balmes, H. Härelind, *ACS Catal.,* 2015, **5**, 6209-6218.

11 S. Sarfraz, A.T. Garcia-Esparza, A. Jedidi, L. Cavallo, K. Takanabe, *ACS Catal.,* 2016, **6**, 2842-2851.